AIMS Mathematics, 7(10): 19415–19439.
DOI:10.3934/math.20221066
Received: 01 July 2022
Revised: 17 August 2022
Accepted: 30 August 2022
Published: 02 September 2022

http://www.aimspress.com/journal/Math

Research article

Biological emergent properties in non-spiking neural networks

Loïs Naudin*

Laboratoire Lorrain de Recherche en Informatique et ses Applications, CNRS, Université de Lorraine, Nancy, France

* **Correspondence:** Email: lois.naudin@gmail.com.

Abstract: A central goal of neuroscience is to understand the way nervous systems work to produce behavior. Experimental measurements in freely moving animals (*e.g.* in the *C. elegans* worm) suggest that ON- and OFF-states in non-spiking nervous tissues underlie many physiological behaviors. Such states are defined by the collective activity of non-spiking neurons with correlated up- and down-states of their membrane potentials. How these network states emerge from the intrinsic neuron dynamics and their couplings remains unclear. In this paper, we develop a rigorous mathematical framework for better understanding their emergence. To that end, we use a recent simple phenomenological model capable of reproducing the experimental behavior of non-spiking neurons. The analysis of the stationary points and the bifurcation dynamics of this model are performed. Then, we give mathematical conditions to monitor the impact of network activity on intrinsic neuron properties. From then on, we highlight that ON- and OFF-states in non-spiking coupled neurons could be a consequence of bistable synaptic inputs, and not of intrinsic neuron dynamics. In other words, the apparent up- and down-states in the neuron's bimodal voltage distribution do not necessarily result from an intrinsic bistability of the cell. Rather, these states could be driven by bistable presynaptic neurons, ubiquitous in non-spiking nervous tissues, which dictate their behaviors to their postsynaptic ones.

Keywords: complex network; neural network; neuron model; non-spiking neurons; bifurcation dynamics; *Caenorhabditis elegans*; retina
Mathematics Subject Classification: 34C23, 37G10, 92-10, 92C20, 92B20

1. Introduction

Spiking neurons and spiking neural networks are the most widely studied cases in computational neuroscience due to their ubiquity in neural processes [1–6]. However, such neurons are not the only information processing component of the nervous system. Indeed, numerous nervous tissues in both vertebrate and invertebrate animals function normally without triggering spikes. Spiking neurons

compress continuous inputs into digital signals for transmitting information via action potentials, while non-spiking neurons do not elicit ones but modulate analog signals (*i.e.* graded potential responses). Specifically, the amplitude and waveform of the action potentials are essentially invariant with respect to the amplitude, duration, and waveform of the stimulus, unlike graded potentials which are stimulus dependent (Figure 1.A) [7].

Many nervous tissues are mostly composed of non-spiking neurons such as vertebrate retina networks [8], the *C. elegans* nervous system [9], many interneurons in insects and crustaceans [10], and motorneurons in the Ascaris worm [11]. Retina has long been the object of attention through the modeling of its several major neuronal classes [12–14]. More recently, efforts to model the neurons of the *C. elegans* worm have been made [15, 16], including the development of general optimization methods to characterize non-spiking neuron behaviors [17, 18]. *C. elegans* is a well-known model organism in neuroscience due to the simplicity of its nervous system, only composed of 302 neurons and about 7000 synaptic connections [19–21]. Despite this simplicity, the *C. elegans* nervous system shares fundamental general neuronal principles with more sophisticated nervous systems, including the human one [22–24].

Two standard non-spiking neuron behaviors exist (Figure 1.B): (i) *near-linear*, with smooth depolarizations or hyperpolarizations from the resting potential, and (ii) *bistable*, with nonlinear transitions between the resting potential and a depolarized potential. Therefore, a bistable cell spontaneously alternates between two membrane plateau potentials: a depolarized potential (up-state) and a relatively hyperpolarized potential (down-state). When the membrane potential is in the up-state (respectively down-state), the neuron is said to be ON (respectively OFF). It is worth noting that many spiking neurons also exhibit such a bistable behavior by triggering action potentials in the up-state, such as mitral cells in olfactory bulb [25], purkinje cells [26], or about 15% of the thalamocortical neurons [27].

Whole-brain calcium imaging of neuronal activity in *C. elegans* [28, 29] reveals that several dozens of non-spiking neurons have biological emergent properties such as collective activity with correlated up- and down-states. The same type of collective behavior, with all-ON and all-OFF network states, has also been observed experimentally in a chemotaxis non-spiking neural network of *C. elegans* by monitoring the intracellular calcium dynamics of its neurons [30]. An important question is to determine whether these ON- and OFF-states of coupled neurons result from the intrinsic bistability of these cells, or whether they reflect bistable synaptic inputs [26]. Indeed, as an example, Purkinje cells exhibit intrinsic bistable dynamics [26], whereas up- and down-states in cortical pyramidal neurons are not intrinsic but induced by the synaptic activity [31].

The aim of this paper is to understand how emergent biological ON- and OFF-states in non-spiking neural networks can emerge from the intrinsic dynamics of neurons and their couplings. To do this, we use a recently developed simple model with dimensionless parameters that is able to reproduce the qualitative behavior of both types of non-spiking neurons: near-linear and bistable. First, we analyse mathematically the stationary points and the bifurcation dynamics of this model applied to the RIM, AIY and AFD neurons of *C. elegans* (Figure 1). In particular, RIM and AIY exhibit a near-linear behavior, while AFD displays a bistable one. On this basis, we then give mathematical conditions for determining whether the up- and down-states in non-spiking neural networks are the result of intrinsic bistability or bistable synaptic activity. Finally, using a canonical example of a network of two coupled neurons, we show that up- and down-states in non-spiking neural networks could be

driven by bistable neurons which dictate their behaviors to their postsynaptic ones through bistable synaptic inputs. The generality of our study gives a rigorous framework for better understanding how the behavior of coupled non-spiking neurons depends on their intrinsic dynamics and their couplings. In other words, it allows to gain insight into how intrinsic dynamics and couplings of single non-spiking neurons impact neural network behaviors.

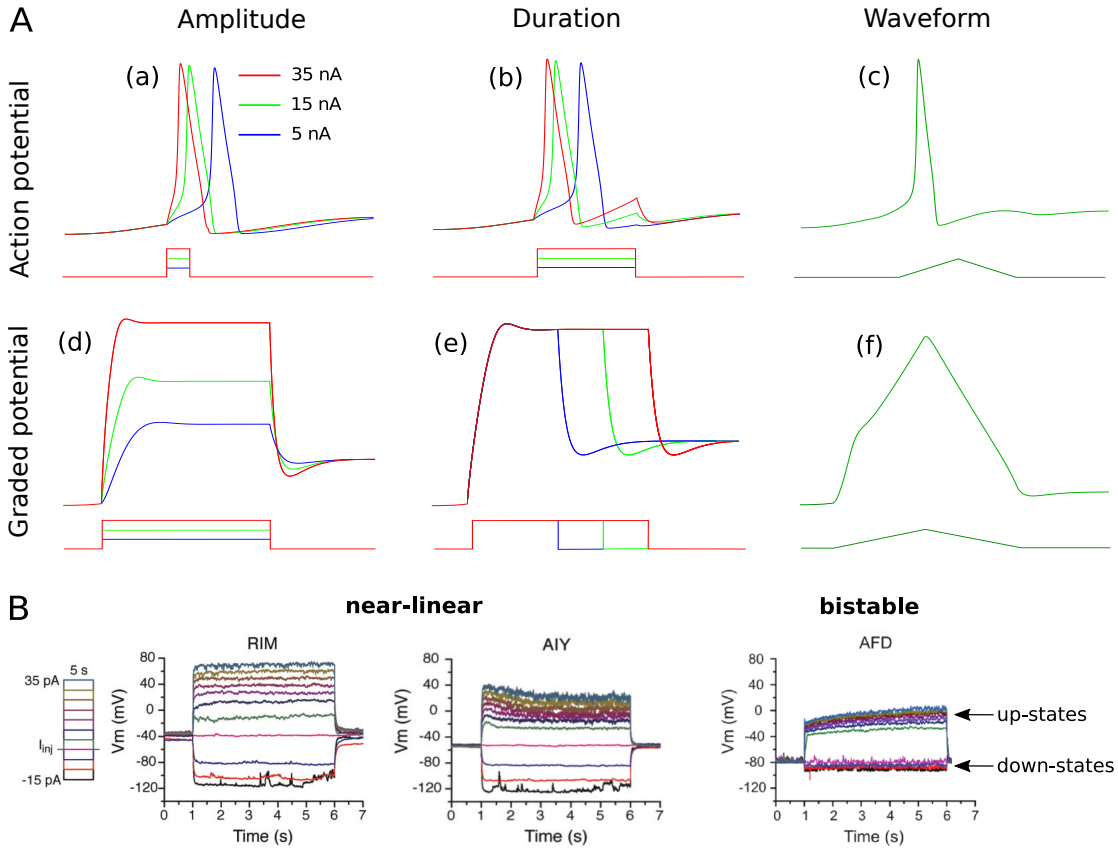

Figure 1. (A) Difference of features between action potentials (a-c) and graded potentials (d-f). Action potentials have been simulated from the classical Hodgkin-Huxley model, while graded potentials have been obtained by reducing its maximal conductances g_{Na} and g_K. The amplitude and waveform of the action potentials are essentially invariant with respect to the (a) amplitude, (b) duration, and (c) waveform of the stimulus. Conversely, the amplitude and waveform of the graded potentials are dependent on the (d) amplitude, (e) duration, and (f) waveform of the stimulus. **(B)** Experimental examples of near-linear (RIM and AIY) and bistable (AFD) non-spiking neurons. The evolution of the membrane potential has been recorded in response to a series of current injections, in the space of 5 seconds, starting from -15 pA and increasing to 35 pA by 5 pA increments. In all cases, the higher the current intensity, the higher the amplitude of the membrane potential. The experimental data have been reproduced from [33] and [17] with the consent of the authors.

The remainder of this paper is organized as follows. Section 2 presents the new non-spiking phenomenological model recently developed in [32]. The analysis of its stationary points and its bifurcation dynamics is carried out in Section 3. Section 4 presents elements for modeling synaptic

connections in non-spiking neural networks, with a particular focus on *C. elegans*. Then, we study both mathematically and numerically how the intrinsic dynamics of a simple presynaptic neuron impact the behavior of a postsynaptic neuron.

2. Presentation of the phenomenological non-spiking model

Non-spiking neurons are ubiquitous in many nervous tissues. For this reason, a recent simple model has been proposed in [32] as an alternative to conductance-based models (a.k.a. Hodgkin–Huxley type models), known to be computationally expensive and difficult to treat mathematically. In this section, we briefly present this simple non-spiking neuron model, derived from the bifurcations' study of conductance-based models (CBMs) of non-spiking neurons [17, 34].

Let V represent the membrane potential of a neuron. The neuron 1-D model takes the general form

$$\tau \frac{dV}{dt} = -f(V) + I \tag{2.1}$$

where I describes an injection current, τ the *constant* time for which V reaches its equilibrium value V_*, and $V \mapsto f(V)$ a cubic function which reads as

$$f(V) = aV^3 + bV^2 + cV + d. \tag{2.2}$$

The parameters a, b, c, and d are dimensionless. These are estimated to reproduce the steady-state current of the neuron, noted I_∞, shown to determine the neuro-computational features of non-spiking neurons [17]. The biological meaning of the steady-state current is the following: in typical voltage-clamp experiments, the membrane potential is clamped at several values V_H (H for hold) for which the resulting currents are measured (Figure 2.A, left). Asymptotic values ($t \to \infty$) of those currents, depending only on V_H, are called steady-state currents (Figure 2.A, right). As a representative example, the experimental steady-state currents of the RIM, AIY and AFD neurons are represented in Figure 9. The stationary points V_* of the model (2.1) satisfy

$$f(V_*) = I$$

so that the function $V \mapsto f(V)$, in particular its shape, determines the neuro-computational features of the non-spiking model (2.1). Indeed, two typical shapes of the curve f exist, monotonic and N-shaped (Figure 2.B), each involving two fundamental different behaviors of the neuron:

- As shown in Figure 2.B (left), a model with a monotonic function f has only one equilibrium for any value of I. Such a model displays a near-linear behavior characterized by smooth depolarizations or hyperpolarizations from the resting potential, such as the RIM and AIY neurons (Figure 1.B, left).
- As shown in Figure 2.B (right), a model with a N-shaped function f has one, two, or three equilibria depending on the value of I. Such a model displays a bistable behavior characterized by voltage jumps between the resting potential and a depolarized potential, such as the AFD neuron (Figure 1.B, right).

In a previous work [32], the parameters of the model (2.1) were estimated using the differential evolution algorithm [35] to fit the experimental steady-state current of the RIM, AIY and AFD neurons

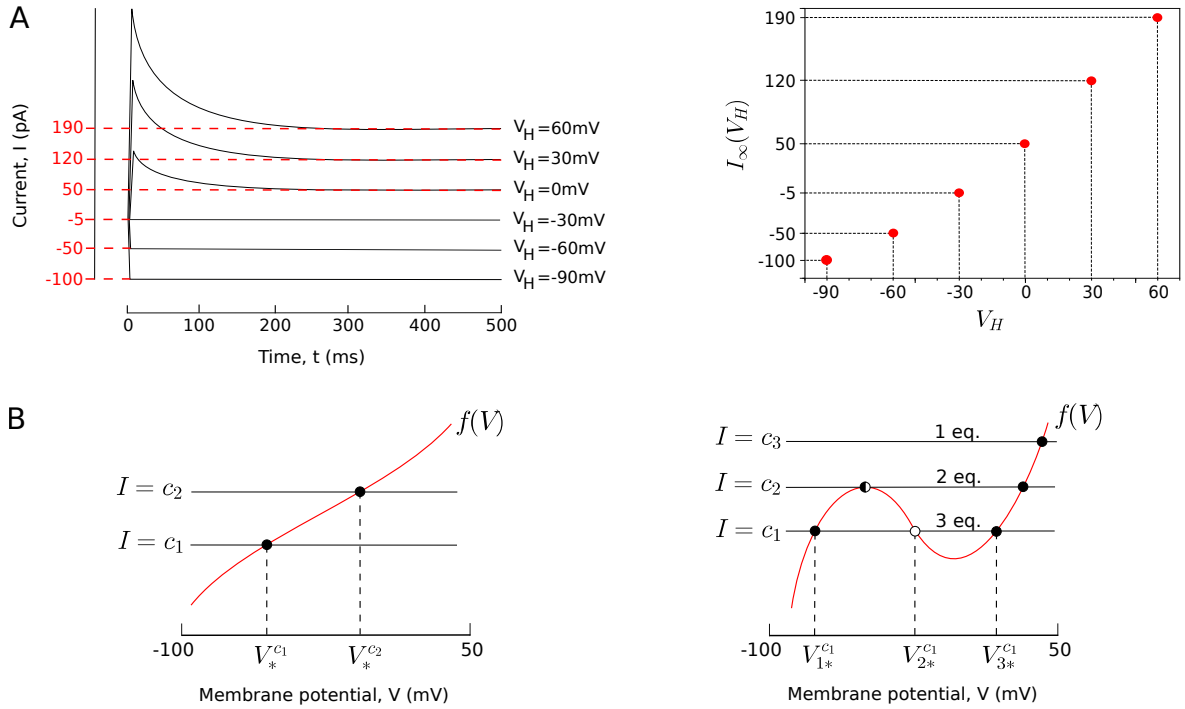

Figure 2. **(A)** (Left) Evolution of the total ion currents of the neuron when its membrane potential is clamped at a fixed value, in spans of 500 milliseconds, from −90 mV and increasing to 60 mV by 30 mV increments. (Right) Steady-state current obtained from the voltage-clamp recordings in (Left). Each value of the steady-state current corresponds to the value of the current of the last milliseconds of each voltage step. **(B)** Two typical shapes of the function f, in red. Intersections of f and horizontal line $I = c$ (with c constant) correspond to equilibria of the system. We denote stable equilibria a as filled circles ●, unstable equilibria as open circles ○ and saddle-node equilibria as ◐. (Left) Monotonic steady-state current. $V_*^{c_1}$ and $V_*^{c_2}$ correspond to equilibria for a current injection $I = c_1$ and $I = c_2$ respectively. (Right) N-shaped steady-state current. The number of equilibria of the system depends on the value of I. For the sake of readibility, we highlight equilibria only for $I = c_1$, noted $V_{1*}^{c_1}$, $V_{2*}^{c_1}$ and $V_{3*}^{c_1}$.

displayed in Figure 9. Further, we reproduced the *mean* of the steady-state current (Figure 3.A) in order to capture the experimental trial-to-trial variability of non-spiking neuron responses, which is known to be larger than that of spiking neurons [36]. Finally, Figure 3.B shows the resulting voltage dynamics of the model against an example of experimental voltage traces. Again, the model is not intended to reproduce the specific shown traces, but to capture the trial-to-trial variability of the neuron responses. As explained in [32], although the model slightly diverges from the experimental voltage traces, it preserves the main qualitative features of the neuron dynamics. Indeed, the RIM model is depolarized or hyperpolarized in a smooth manner under current clamp, while the AIY model is more sensitive to hyperpolarization than depolarization inputs with transition point around −30 mV, as in the experimental membrane potential behaviors. Likewise, the voltage jump of the AFD model to its up-state occurs for the same values of current injections as in the biological neuron.

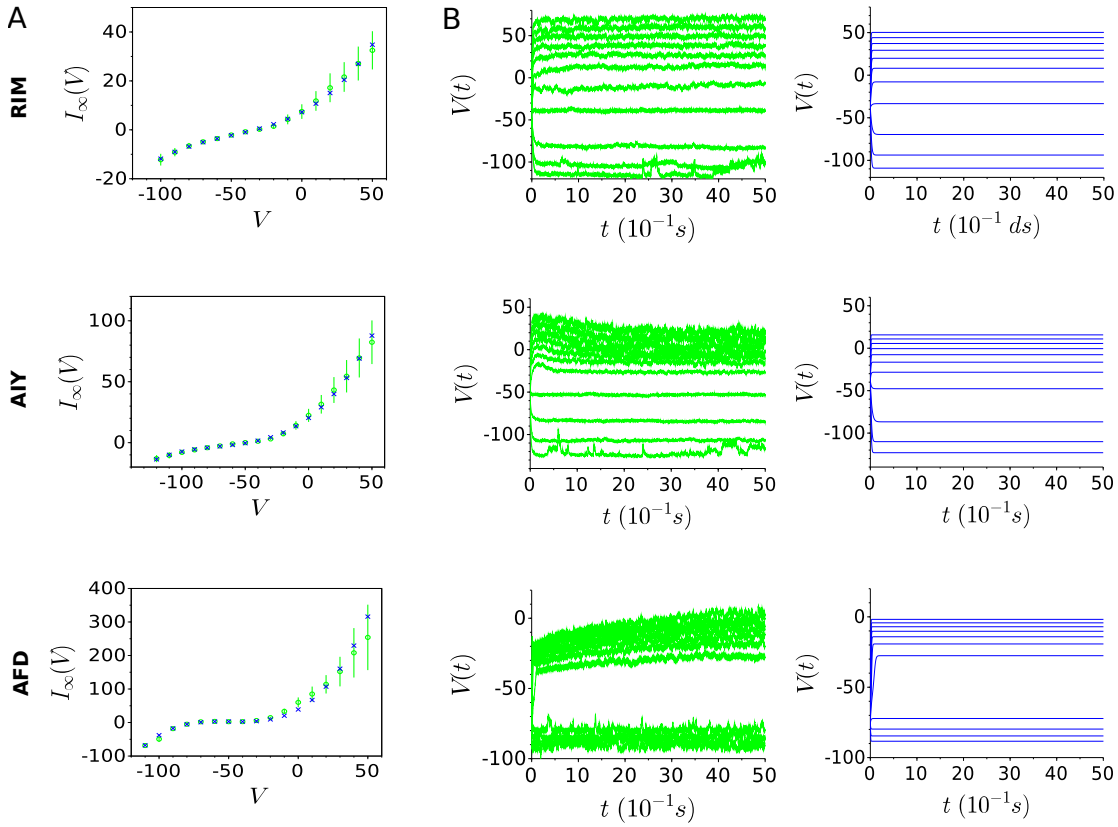

Figure 3. **(A)** Mean of the experimental steady-state current (represented by green circles) with respective error bars, and the estimated steady-state current (represented by blue crosses) given by the equation (2.2) with parameter values displayed in Table 2. **(B)** Example of experimental voltage traces for the RIM, AIY and AFD neurons against their respective models, for injection currents starting from −15 pA and increasing 35 pA by 5 pA increments.

3. Mathematical analysis of the non-spiking model

This section aims at studying the phenomenological non-spiking model (2.1) presented in Section 2. The first part analyses the stationary points of the model, while the second studies its bifurcation dynamics. Moreover, we apply the model with the parameters of the RIM, AIY and AFD neurons (Table 2), representative of known types of behaviors of non-spiking cells: near-linear and bistable. All numerical simulations of the models presented in this article are performed with the function *ode* of the Scilab software. As a first step, some biological hypotheses are formulated and used throughout the manuscript based on experimental studies.

Biological hypotheses throughout the manuscript. Biological cells have limited tolerance to electrical stimulation. This is even more true for the *C. elegans* neurons due to their small size. Beyond a certain threshold, the stimulus bursts the cell. Therefore, we define the range of the neuron functioning, noted $\mathcal{I}$, as follows:

$$I \in \mathcal{I} := [m; M] \tag{3.1}$$

where $m = -15$ pA and $M = 35$ pA as in [33].

3.1. Stationary point analysis of the model

Let a, b, c and d be the parameters of the model (2.1). In the following, let A and B be defined by

$$\begin{cases} A := \dfrac{27}{a^2} \\ B := \dfrac{54d}{a^2} + \dfrac{54}{a}\left(\dfrac{2b^3}{27a^3} - \dfrac{bc}{3a^2}\right) \end{cases} \tag{3.2}$$

so that

$$\tilde{I} := \frac{B}{2A} \tag{3.3}$$

Moreover, let p and q be defined by

$$\begin{cases} p := -\dfrac{b^2}{3a^2} + \dfrac{c}{a} \\ q(I) := \dfrac{2b^3}{27a^3} - \dfrac{bc}{3a^2} + \dfrac{d-I}{a} \end{cases} \tag{3.4}$$

and I_1 and I_2 as follows:

$$\begin{cases} I_1 := \dfrac{B + \sqrt{B^2 - 4AC}}{2A} \\ I_2 := \dfrac{B - \sqrt{B^2 - 4AC}}{2A} \end{cases} \tag{3.5}$$

where

$$C = 27\left(\frac{2b^3}{27a^3} - \frac{bc}{3a^2}\right)^2 + \frac{54d}{a}\left(\frac{2b^3}{27a^3} - \frac{bc}{3a^2}\right) + \frac{27d^2}{a^2} + 4p^3 \tag{3.6}$$

Then, the following proposition holds.

Proposition 3.1. *Let*

$$\Delta(I) := 4p^3 + 27q^2(I) \tag{3.7}$$

where p and q are defined in (3.4)*. Moreover, let $\tilde{I}$ be defined by* (3.3)*, and I_1 and I_2 be defined by* (3.5)*. Then:*

1. *if $\Delta(\tilde{I}) > 0$, the model* (2.1) *has a unique stationary point $V_*(I)$ for all $I \in \mathcal{I}$ given by*

$$V_*(I) = \sqrt[3]{-\frac{q(I)}{2} + \sqrt{\frac{q^2(I)}{4} + \frac{p^3}{27}}} + \sqrt[3]{-\frac{q(I)}{2} - \sqrt{\frac{q^2(I)}{4} + \frac{p^3}{27}}} \tag{3.8}$$

2. *if $\Delta(\tilde{I}) \leq 0$, then:*
   - *for all $I \in]m; I_1[\cup]I_2; M[$, the model* (2.1) *has a unique stationary point $V_*(I)$ given in* (3.8)*.*

- *for $I = I_1$ and $I = I_2$, the model* (2.1) *has two stationary points $V_{1*}(I)$ and $V_{2*}(I)$ given by*

$$\begin{cases} V_{1*}(I) = 2\sqrt[3]{-\dfrac{q(I)}{2}} \\ V_{2*}(I) = -\sqrt[3]{-\dfrac{q(I)}{2}} \end{cases} \tag{3.9}$$

- *for all $I \in]I_1; I_2[$, the model* (2.1) *has three stationary points $V_{1*}(I)$, $V_{2*}(I)$ and $V_{3*}(I)$ given by*

$$\begin{cases} V_{1*}(I) = \sqrt{-\dfrac{4p}{3}}\sin\left(\dfrac{\rho}{3}\right) \\ V_{2*}(I) = \sqrt{-\dfrac{4p}{3}}\sin\left(\dfrac{2\pi+\rho}{3}\right) \\ V_{3*}(I) = \sqrt{-\dfrac{4p}{3}}\sin\left(\dfrac{4\pi+\rho}{3}\right) \end{cases} \tag{3.10}$$

where $\rho = \arcsin\left(\sqrt{-\dfrac{27q^2(I)}{4p^3}}\right)$.

Proof. The stationary points of the model (2.1) are given by solving

$$aV^3 + bV^2 + cV + d - I = 0 \tag{3.11}$$

Let us denote $V = X - \alpha/3$ with $\alpha = b/a$. Then, the equation (3.11) can be rewritten as

$$X^3 + pX + q = 0 \tag{3.12}$$

where p and q are defined in (3.4). The number of roots of the third-degree polynomial (3.12) depends on the sign of the function Δ defined in (3.7) which is its discriminant. Moreover, Δ is a convex parabola, so that the number of stationary points of the model (2.1) is determined by the sign of the minimum of the function Δ. We can rewrite Δ in the following form:

$$\Delta(I) = AI^2 - BI + C \tag{3.13}$$

where A and B are defined in (3.2), and C is defined in (3.6). Then, we have

$$\Delta'(I) = 2AI - B = 0 \quad \Longleftrightarrow \quad I = \frac{B}{2A}$$

so that the minimum of the function Δ is reached in $\tilde{I} = B/2A$. From the Cardan-Tartaglia method, if $\Delta(\tilde{I}) > 0$ then the model (2.1) displays a unique stationary point given by the equation (3.8). Moreover, if $\Delta(\tilde{I}) \leq 0$, then the model (2.1) has one, two, or three stationary points depending on the value of I. The critical values of I at which the number of stationary points changes are those satisfying $\Delta(I) = 0$. These are given by I_1 and I_2 defined in (3.5). Therefore, for all $I < I_1$ and $I > I_2$, $\Delta(I) > 0$ so that we have only one stationary point given by (3.8); for $I = I_1$ or $I = I_2$, $\Delta(I) = 0$ so that we have two stationary points given by (3.9); for all $I_1 < I < I_2$, $\Delta(I) < 0$ so that we have three stationary points given by (3.10). □

Biological interpretation. If $\Delta(\tilde{I}) > 0$, then the model (2.1) displays a near-linear behavior defined by smooth depolarizations or hyperpolarizations from the resting potential (Figure 1.B, left). If $\Delta(\tilde{I}) < 0$, then the model (2.1) exhibits a bistable behavior defined by a nonlinear transition between the resting potential and a depolarized potential (Figure 1.B, right). In this case, I_1 and I_2 defined in (3.5) are the injection current thresholds from which the neuron jumps to its down- and up-state, respectively.

Application to the RIM, AIY and AFD neurons. Here we determine the number and the expression of the stationary points of the three neurons under study (RIM, AIY and AFD). To do this, we compute $\Delta(\tilde{I})$, defined in (3.7), with the parameters a, b, c and d given in Table 2, determined in a previous work [32] to reproduce the qualitative behavior of these neurons. The result for each ones is summarized in Table 1 and shown in Figure 4.

Table 1. Minimum of the function $I \mapsto \Delta(I)$ for each neuron.

Neuron	**RIM**	**AIY**	**AFD**
$\Delta(\tilde{I})$	6.18e11	6.27e10	-1.57e07

We observe that $\Delta(\tilde{I}) > 0$ for the RIM and AIY neurons so that the following corollary holds from Proposition 3.1.

Corollary 3.1 (RIM and AIY neurons)**.** *Model* (2.1) *endowed with parameters values relative to the RIM and AIY neurons has a unique stationary point V_* given in* (3.8)*.*

Moreover, $\Delta(\tilde{I}) < 0$ for the AFD neuron. We compute I_1 and I_2 defined in (3.5) and we find $I_1 = 2.62$ and $I_2 = 3.12$. Then, we have the following corollary:

Corollary 3.2 (AFD neuron)**.** *Let $I_1 = 2.62$ and $I_2 = 3.12$. Then, model* (2.1) *endowed with parameters values relative to the AFD neuron displays one, two, or three stationary points depending on the value of I:*

- *for all $I \in]m; I_1[\cup]I_2; M[$, AFD has a unique stationary point $V_*(I)$ given in* (3.8)*;*
- *for $I = I_1$ and $I = I_2$, AFD has two stationary points $V_{1*}(I)$ and $V_{2*}(I)$ given in* (3.9)*;*
- *for all $I \in]I_1; I_2[$, AFD has three stationary points $V_{1*}(I)$, $V_{2*}(I)$ and $V_{3*}(I)$ given in* (3.10)*.*

Stability of stationary points. Consider I such as $F(V_*(I), I) = 0$ where F is the right-hand side of the model (2.1). The first-order derivative of the function $(V, I) \mapsto F(V, I)$ with respect to V is given by

$$\frac{\partial F(V,I)}{\partial V} = -3aV^2 - 2bV - c \tag{3.14}$$

Then, for each neuron, we compute from Cardan-Tartaglia formula the equilibria $V_*(I)$ for each $I \in \mathcal{I}$ by 0.01pA, as well as the value of the function (3.14) in $V_*(I)$ to determine its nature. As shown in Figure 5, the sign of the function (3.14) is always negative for RIM and AIY, showing that their unique equilibrium point is always stable. Regarding AFD, it depends on the value of I. For any $I < I_1$ and $I > I_2$, the unique equilibrium point is stable. For $I = I_1$ and $I = I_2$, we have one stable and one non-hyperbolic equilibrium point. For any $I \in]I_1; I_2[$, we have two stable equilibria and one unstable equilibrium point.

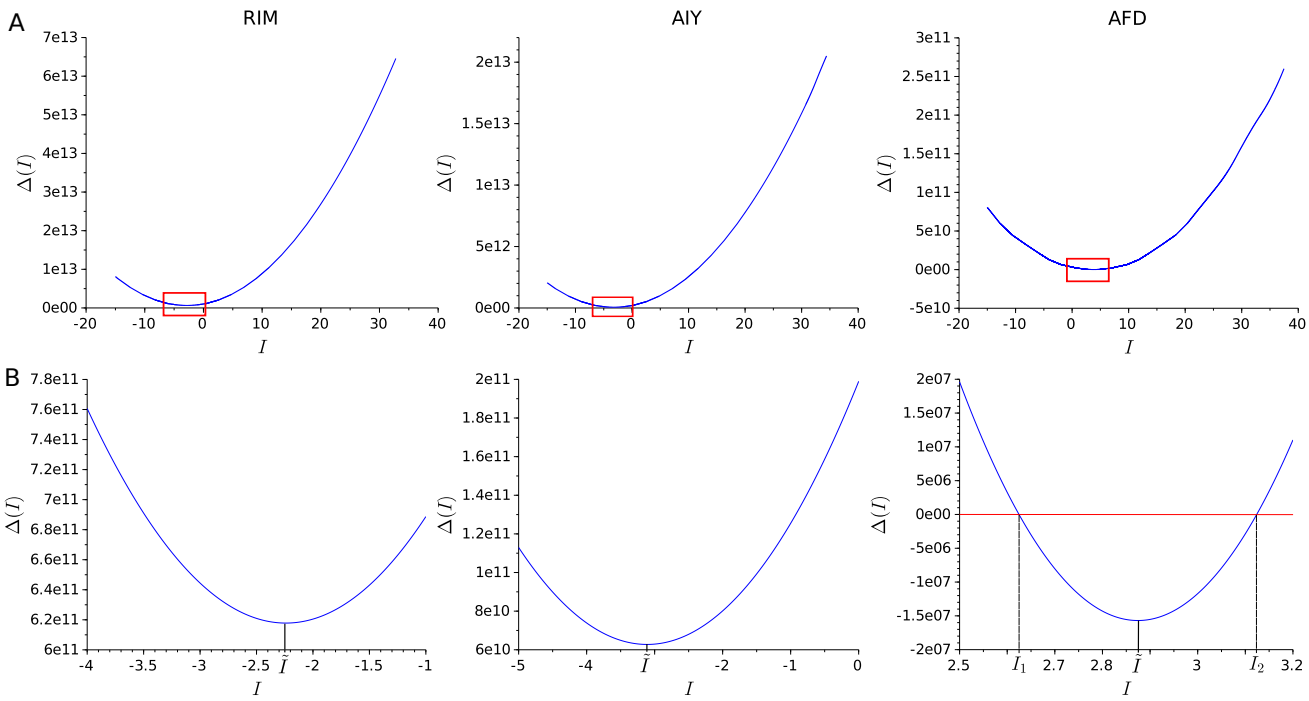

Figure 4. Dynamics of the function $I \mapsto \Delta(I)$ for the RIM, AIY and AFD neurons. **(A)** Dynamics of $I \mapsto \Delta(I)$ for all $I \in \mathcal{I}$ where $\mathcal{I}$ is defined in (3.1). **(B)** Zoom of the red box displayed in (A). The sign of the function Δ for RIM and AIY is always positive, implying a unique equilibrium point for all values of I. For AFD, the sign of Δ depends on the value of I: for all $I < I_1$ and $I > I_2$, $\Delta(I) > 0$ (so a unique equilibrium point); for all $I_1 < I < I_2$, $\Delta(I) < 0$ (so three equilibria); and for $I = I_1$ and $I = I_2$, $\Delta(I) = 0$ (so two equilibria). $\tilde{I}$ denotes the argmin of the function Δ.

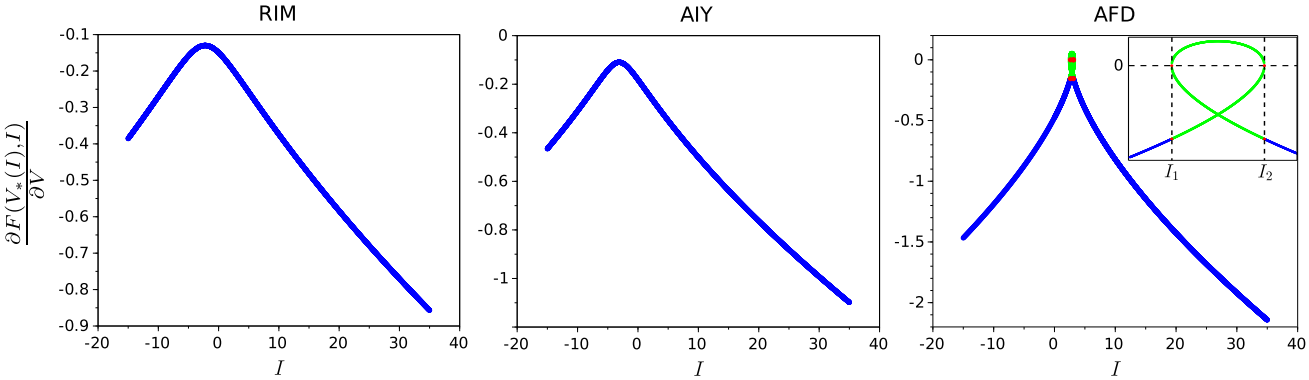

Figure 5. Stability of equilibria for the RIM, AIY and AFD neurons. For RIM and AIY, the sign of the first-order derivative of the function F defined in (3.14) with respect to V is always negative for all $I \in \mathcal{I}$, so that their unique equilibrium point is stable. For AFD, the sign is negative for $I < I_1$, so for these values of injection currents, the single equilibrium point is stable. For $I = I_1$ and $I = I_2$, we have two equilibria, one stable and one non-hyperbolic. For $I \in]I_1, I_2[$, we have three equilibria, two stable and one unstable.

3.2. Bifurcation analysis of the model

The analysis of the stationary points carried out in the previous section shows the existence of two non-hyperbolic equilibrium points for bistable dynamics of the model (2.1). The following proposition gives information on the dynamics of the model (2.1) near these points.

Proposition 3.2. *Let $V_*(I_*)$ be a non-hyperbolic equilibrium point of the model* (2.1) *such as*

$$3aV_* + b \neq 0.$$

Then, a saddle-node bifurcation occurs at $I = I_*$.
Moreover, the normal form of the model (2.1) *near the stationary point $V_*(I_*)$ is given by*

$$\begin{cases} \dfrac{d\eta}{dt} = \mu - \eta^2 & \text{if} \quad 3aV_* + b > 0 \\ \dfrac{d\eta}{dt} = \mu + \eta^2 & \text{if} \quad 3aV_* + b < 0 \end{cases} \tag{3.15}$$

where

$$\mu = |3aV_* + b|(I - I_*)$$

Proof. For the convenience of readability, we set $\tau = 1$.

- We carry out the following change of variables:

$$\begin{cases} y = V - V_* \\ p = I - I_* \end{cases}$$

The model (2.1) in the new coordinates becomes

$$\begin{aligned} \frac{dy}{dt} &= -a(y + V_*)^3 - b(y + V_*)^2 - c(y + V_*) - d + p + I_* \\ &= -ay^3 - 3aV_*y^2 - 3aV_*^2y - aV_*^3 - by^2 - 2bV_*y - bV_*^2 - cy - cV_* - d + p + I_* \\ &:= g(y, p) \end{aligned} \tag{3.16}$$

Therefore, $(0, 0)$ is a non-hyperbolic stationary point of the model (3.16).

- The third order term in y is negligible in 0 compared to the second order and first order terms in y. Then, we obtain

$$\begin{aligned} \frac{dy}{dt} &= -3aV_*y^2 - 3aV_*^2y - aV_*^3 - by^2 - 2bV_*y - bV_*^2 - cy - cV_* - d + p + I_* \\ &= (-3aV_* - b)y^2 + (-3aV_*^2 - 2bV_* - c)y - aV_*^3 - bV_*^2 - cV_* - d + I_* + p \end{aligned} \tag{3.17}$$

Given

$$-3aV_*^2 - 2bV_* - c = \frac{\partial g}{\partial y}(0, 0) = 0$$

and

$$-aV_*^3 - bV_*^2 - cV_* - d + I_* = g(0,0) = 0$$

the Eq (3.17) becomes

$$\frac{dy}{dt} = (-3aV_* - b)y^2 + p$$

By assumption, $-3aV_* - b \neq 0$, so that

$$\begin{cases} \dfrac{dy}{dt} = p - (3aV_* + b)y^2 & \text{if} \quad 3aV_* + b > 0 \\ \dfrac{dy}{dt} = p + |3aV_* + b|y^2 & \text{if} \quad 3aV_* + b < 0 \end{cases} \tag{3.18}$$

- Finally, we rescale the Eqs (3.18) by considering the change of variable

$$\eta = |3aV_* + b|y$$

so that

$$\begin{cases} \dfrac{d\eta}{dt} = \mu - \eta^2 & \text{si} \quad 3aV_* + b > 0 \\ \dfrac{d\eta}{dt} = \mu + \eta^2 & \text{si} \quad 3aV_* + b < 0 \end{cases}$$

where

$$\mu = |3aV_* + b|p$$

□

Application to the AFD neuron. In the previous section, we highlighted two non-hyperbolic equilibrium points $V_*(I_1)$ and $V_*(I_2)$ in the case of the AFD neuron (see Figure 5 as an illustration), where I_1 and I_2 are still defined in (3.5). Indeed,

$$\frac{\partial F(V_*(I_1), I_1)}{\partial V} = 0 \quad \text{and} \quad \frac{\partial F(V_*(I_2), I_2)}{\partial V} = 0$$

where F is given in (3.14). From Proposition 3.2, the dynamics of the model (2.1) near the non-hyperbolic equilibrium $V_*(I_1)$ is given by the following normal form:

$$\frac{d\eta}{dt} = \mu - \eta^2 \tag{3.19}$$

whereas near $V_*(I_2)$, the normal form reads as

$$\frac{d\eta}{dt} = \mu + \eta^2. \tag{3.20}$$

Finally, we obtain the bifurcation diagram displayed in Figure 6.

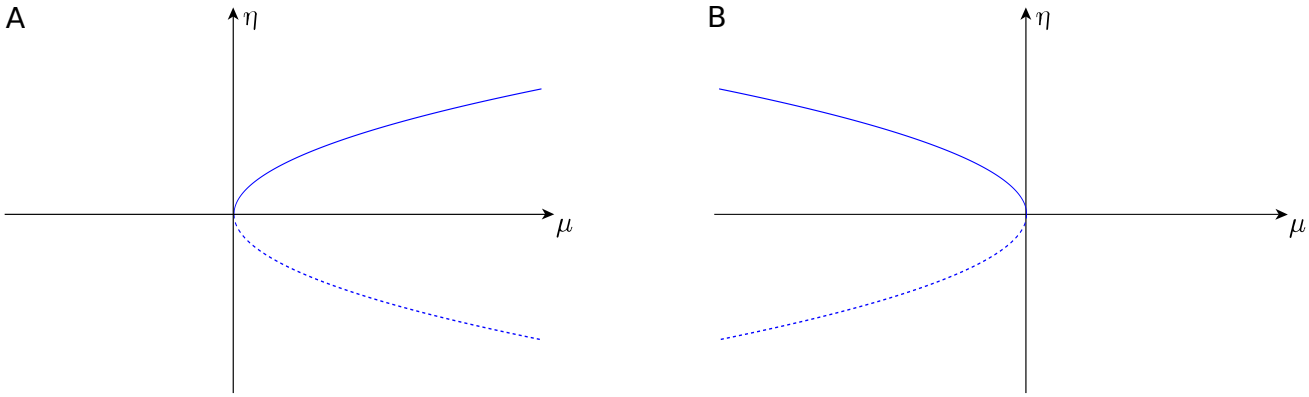

Figure 6. Saddle-node bifurcation diagram **(A)** near the non-hyperbolic stationary point $V_*(I_1)$, and **(B)** near the non-hyperbolic stationary point $V_*(I_2)$.

4. Non-spiking neural network

Experimental measurements of the non-spiking neuronal activity in freely *C. elegans* worms show that ON and OFF network states underlie physiological behaviors [28–30]. This section aims at understanding how such correlated up- and down-states of the membrane potential of the neurons can emerge from the intrinsic neuron dynamics and their couplings. To that end, we first present the *C. elegans* synaptic connections and their modeling, before determining mathematical conditions informing whether the ON- and OFF-states result from the intrinsic neuron dynamics or the synaptic activity.

4.1. C. elegans synaptic connection

Anatomical reconstruction of the *C. elegans* nervous system reveals both chemical and electrical synaptic connections [37]. Synaptic transmission at chemical synapses occurs through the release of neurotransmitters similar to those in more complex vertebrates, such as GABA [38], glutamate [39], acetylcholine [40], and some amines (serotonine, dopamine, etc.) [41]. Regarding *C. elegans* gap junctions [42], *i.e.* electrical synapses, numerous works demonstrate their functional equivalence to mammalian gap junctions (we refer to [43] for a recent review). Chemical and eletrical synapses often coexist in same target neurons.

From a general viewpoint, neurons can transmit information through various modes of neurotransmitter release. In the case of *C. elegans*, experimental biological studies show that neurons release neurotransmitters in a graded manner [44–48]. In addition, there is evidence of a graded release in *Ascaris lumbricoides* [49, 50], another extensively studied nematode related to *C. elegans*. More precisely, the graded synaptic connection is defined as follows:

Definition 4.1 (Graded synaptic connection [45])**.** *Graded synaptic connection is one in which action potentials are required neither for transmitter release nor for postsynaptic signalling, and in which incremental changes in membrane potential in the soma of the presynaptic neuron cause incremental changes in membrane potential in the soma of the postsynaptic neuron.*

Graded release of neurotransmitters in *C. elegans* has been firstly modeled in [51] based on data from *Ascaris lumbricoides* [49, 50] adapted to the particular case of *C. elegans* neurons. In the

following, we will refine some parameter values based on recent experimental evidences from *C. elegans*.

4.2. Modeling of synaptic connections

Each instance of the models composing the network follow the general equation

$$\tau_i \frac{dV_i}{dt} = -f(V_i) - \sum_{j=1}^{N} (I_{ij}^{syn} + I_{ij}^{gap}) + I_i^{ext} \tag{4.1}$$

with

$$f(V_i) = a_i V_i^3 + b_i V_i^2 + c_i V_i + d_i$$

where:

- V_i denotes the membrane potential of a neuron i;
- τ_i, a_i, b_i, c_i, and d_i are the parameters of the neuron i;
- N is the number of neurons in the network;
- I_i^{ext} is any injected current by the experimenter, modeling a sensory input;
- I_{ij}^{syn} is the synaptic current flowing into neuron i from neuron j accross a single chemical synapse;
- I_{ij}^{gap} the current flowing across a single gap junction between neuron j and neuron i.

Gap junctions are modeled as ohhmic resistances, while channels of chemical synapses are gated in the postsynaptic membrane with inward current. Their respective expressions are therefore given by

$$I_{ij}^{gap} = g_{ij}^{gap}(V_i - V_j)$$

$$I_{ij}^{syn} = g_{ij}(t)(V_i - E_{ij})$$

with:

- E_{ij} the reversal potential for the synaptic conductance, set to 0mV for excitatory synapses and −48mV for inhibitory synapses [51];
- V_j a presynaptic membrane potential;
- g_{ij}^{gap} the *constant* conductance of the gap junction. Recent experimental works [52, 53] directly recorded trans-junctional currents between *C. elegans* neurons, from AVA to VA5, giving a parameter value to about 0.4nS. Therefore, g_{ij}^{gap} will be set to 0.4;
- g_{ij} the synaptic conductance of the postsynaptic membrane which is gated according to presynaptic potential V_j of a sigmoidal manner. Therefore, $t \mapsto g_{ij}(t)$ is described by the equation

$$\frac{dg_{ij}}{dt} = \frac{g_{ij\infty}(V_j) - g_{ij}}{\tau_{ij}}$$

  where τ_{ij} is the synaptic constant time and $V \mapsto g_{ij\infty}(V)$ is a sigmoidal function relating pre- and postsynaptic membrane potential. In the *C. elegans* worm, $\tau_{ij} \ll 1$, so that the activation of synaptic conductances can be considered as instantaneous [51]. Therefore, the synaptic conductances depend only on the presynaptic membrane potential V_j, *i.e.*

$$g_{ij}(t) = g_{ij\infty}(V_j)$$

Finally, the expression of $g_{ij\infty}$ is given by

$$g_{ij\infty}(V_j) = \frac{\overline{g}_{ij}}{1 + \exp\left(\frac{V_{1/2}^{ij} - V_j}{V_{slope}}\right)}$$

where $\overline{g}_{ij}$ is the maximal postsynaptic conductance, $V_{1/2}^{ij}$ satisfies $g_{ij\infty}(V_{1/2}^{ij}) = \overline{g}_{ij}/2$, and V_{slope} the slope factor where smaller values of V_{slope} lead to a sharper $g_{ij\infty}$.

In the following section, we carry out a mathematical analysis of the dynamics of coupled neurons based on the formalism described in this section.

4.3. Mathematical analysis of coupled non-spiking neurons

Let N be the number of neurons in the network, and $i \in \{1, \ldots, N\}$ a given neuron. Based on the previous section, the dynamics of the membrane potential of the neuron i is given by

$$\tau_i \frac{dV_i}{dt} = -f(V_i) - \sum_{j=1}^{N} \underbrace{g_{ij\infty}(V_j)(V_i - E_{ij})}_{I_{ij}^{syn}} - \sum_{j=1}^{N} \underbrace{g_{ij}^{gap}(V_i - V_j)}_{I_{ij}^{gap}} + I_i^{ext} \tag{4.2}$$

where

$$g_{ij\infty}(V_j) = \frac{\overline{g}_{ij}}{1 + \exp\left(\frac{V_{1/2}^{ij} - V_j}{V_{slope}}\right)}$$

and

$$f(V_i) = a_i V_i^3 + b_i V_i^2 + c_i V_i + d_i.$$

Therefore, the system (4.2) can be written as follows:

$$\tau_i \frac{dV_i}{dt} = -a_i V_i^3 - b_i V_i^2 - C_i(V_j) V_i - \mathcal{D}_i(V_j, I_i^{ext}) \tag{4.3}$$

where

$$\begin{cases} C_i(V_j) = c_i + \sum_{j=1}^{N} g_{ij}^{gap} + \sum_{j=1}^{N} g_{ij\infty}(V_j) \\ \mathcal{D}_i(V_j, I_i^{ext}) = d_i - \sum_{j=1}^{N} g_{ij\infty}(V_j) E_{ij} - \sum_{j=1}^{N} g_{ij}^{gap} V_j - I_i^{ext} \end{cases}$$

Stationary point analysis of the coupled models. From (4.3), the stationary points of the membrane potential of the neuron i verify

$$a_i V_i^3 + b_i V_i^2 + C_i(V_j) V_i + \mathcal{D}_i(V_j, I_i^{ext}) = 0 \tag{4.4}$$

where V_j and I_i^{ext} are considered as parameters of the system of the neuron i. Then, based on the previous section, the discriminant of the third-degree polynomial (4.4) is given by

$$\Delta_i(V_j, I_i^{ext}) = 4p_i(V_j)^3 + 27q_i^2(V_j, I_i^{ext}) \tag{4.5}$$

where

$$\begin{cases} p_i(V_j) := -\dfrac{b_i^2}{3a_i^2} + \dfrac{C_i(V_j)}{a_i} \\ q_i(V_j, I_i^{ext}) := \dfrac{2b_i^3}{27a_i^3} - \dfrac{b_iC_i(V_j)}{3a_i^2} + \dfrac{\mathcal{D}_i(V_j, I_i^{ext})}{a_i} \end{cases} \tag{4.6}$$

where C_i and $\mathcal{D}_i$ are defined in (4.3). Then, the following proposition holds.

Proposition 4.1. *Let Δ_i be defined in* (4.5)*, p_i and q_i be defined in* (4.6)*, and V_j and I_i^{ext} be the inputs considered as parameters. Then:*

- *if $\Delta_i > 0$, the membrane potential of the neuron i has a unique stationary point $V_i^*(V_j, I_i^{ext})$ given by*

$$V_i^*(V_j, I_i^{ext}) = \sqrt[3]{-\frac{q_i(V_j, I_i^{ext})}{2} + \sqrt{\frac{q_i^2(V_j, I_i^{ext})}{4} + \frac{p_i^3(V_j)}{27}}} + \sqrt[3]{-\frac{q_i(V_j, I_i^{ext})}{2} - \sqrt{\frac{q_i^2(V_j, I_i^{ext})}{4} + \frac{p_i^3(V_j)}{27}}}$$

- *if $\Delta_i = 0$, the membrane potential of the neuron i exhibits two stationary points $V_i^{1*}(V_j, I_i^{ext})$ and $V_i^{2*}(V_j, I_i^{ext})$ which reads as*

$$\begin{cases} V_i^{1*}(V_j, I_i^{ext}) = 2\sqrt[3]{-\dfrac{q_i(V_j, I_i^{ext})}{2}} \\ V_i^{2*}(V_j, I_i^{ext}) = -\sqrt[3]{-\dfrac{q_i(V_j, I_i^{ext})}{2}} \end{cases}$$

- *if $\Delta_i < 0$, the membrane potential of the neuron i has three stationary points $V_i^{1*}(V_j, I_i^{ext})$, $V_i^{2*}(V_j, I_i^{ext})$ and $V_i^{3*}(V_j, I_i^{ext})$ given by*

$$\begin{cases} V_i^{1*}(V_j, I_i^{ext}) = \sqrt{-\dfrac{4p_i(V_j)}{3}} \sin\Big(\dfrac{\rho_i(V_j, I_i^{ext})}{3}\Big) \\ V_i^{2*}(V_j, I_i^{ext}) = \sqrt{-\dfrac{4p_i(V_j)}{3}} \sin\Big(\dfrac{2\pi + \rho_i(V_j, I_i^{ext})}{3}\Big) \\ V_i^{3*}(V_j, I_i^{ext}) = \sqrt{-\dfrac{4p_i(V_j)}{3}} \sin\Big(\dfrac{4\pi + \rho_i(V_j, I_i^{ext})}{3}\Big) \end{cases}$$

where $\rho_i(V_j, I_i^{ext}) = \arcsin\left(\sqrt{-\dfrac{27q_i^2(V_j, I_i^{ext})}{4p_i^3(V_j)}}\right)$.

Biological interpretation. Beyond informing us about the stationary points of a coupled neuron, Proposition 4.1 tells us about how the coupling impacts the instrinsic dynamics of the coupled neurons. Indeed, if $\Delta_i > 0$, then the neuron i governed by the equation (4.2) displays a near-linear intrinsic dynamics, while it exhibits an intrinsic bistable one if $\Delta_i < 0$.

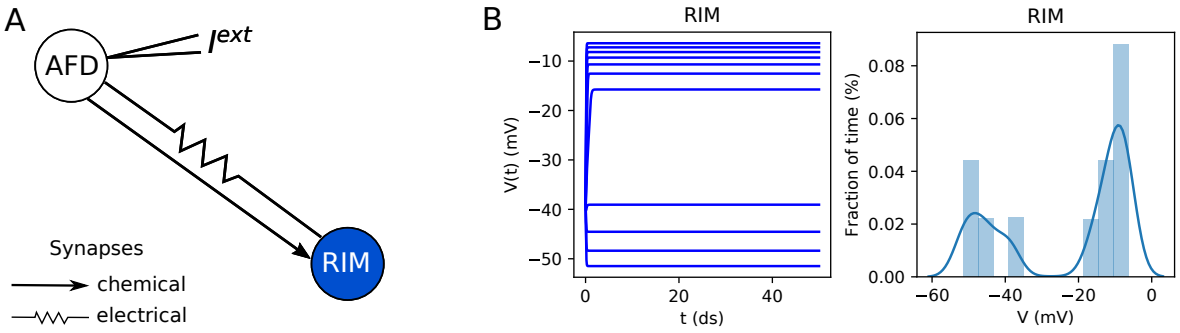

Figure 7. Voltage dynamics of the RIM neuron coupled with the AFD bistable presynaptic neuron. **(A)** Diagram of connectivity between the AFD bistable presynaptic neuron and the RIM near-linear postsynaptic neuron. **(B)** Left: Evolution of the membrane potential of the RIM neuron when its AFD bistable presynaptic neuron is stimulated by a series of injection currents I^{ext}, from −15 pA to 35 pA by 5 pA increments. Right: Corresponding histogram of the membrane potential calculated from 50 ds (5000 ms) of simulation.

Application on a canonical example of two coupled neurons. Here we implement a non-spiking neural network of two coupled neurons through a gap junction and an excitatory chemical synapse (Figure 7.A). We consider the AFD bistable neuron as the presynaptic sensory neuron, noted A, and the RIM near-linear neuron as the postsynaptic neuron, noted R. It is worth noting that the behavior of the AFD and RIM neurons represents the two qualitative types of non-spiking behavior (bistable and near-linear), and are representative of two major quantitative classes of *C. elegans* neurons [33].

The mathematical expression of the network is given by

$$\begin{cases} \tau_A \dfrac{dV_A}{dt} = -a_A V_A^3 - b_A V_A^2 - c_A V_A - d_A + I_A^{ext} \\ \tau_R \dfrac{dV_R}{dt} = -a_R V_R^3 - b_R V_R^2 - c_R V_R - d_R - g_{RA\infty}(V_A)(V_R - E_{RA}) - g_{RA}^{gap}(V_R - V_A) \end{cases}$$

The dynamics of the membrane potential V_R of the RIM neuron shows up- and down-states when coupled with a bistable presynaptic neuron (Figure 7.B, left), as previously reported in [32]. These up- and down-states are apparent in the bimodal distribution of the membrane potential (Figure 7.B, right), computed using the *distplot* function of the Seaborn library in Python. This is in agreement with its bistable intracellular calcium dynamics when exposed to odor stimuli [30]. This shows that the connectivity strongly affects the behavior of RIM: the membrane potential of a near-linear neuron can have bimodal dynamics when coupled with a bistable neuron. The question that then arises is whether these up- and down-states result from the intrinsic bistability of the cell, or whether they reflect bistable synaptic inputs. In other words, we want to understand whether the connectivity has modified the intrinsic nature of the RIM neuron, from a near-linear type to a bistable type. To address

this issue, we use the Proposition 4.1. As a first step, the equation on the postsynaptic RIM neuron is rewritten in the form (4.3):

$$\begin{aligned}\tau_R \frac{dV_R}{dt} = &- a_R V_R^3 - b_R V_R^2 - \overbrace{(c_R + g_{RA\infty}(V_A) + g_{RA}^{gap})}^{C_R(V_A)} V_R \\ &- \underbrace{(d_R - g_{RA\infty}(V_A) E_{RA} - g_{RA}^{gap} V_A)}_{\mathcal{D}_R(V_A, 0)}\end{aligned} \tag{4.7}$$

As the chemical synapse is excitatory, we have $E_{RA} = 0$ so that

$$\begin{cases} C_R(V_A) = c_R + g_{RA\infty}(V_A) + g_{RA}^{gap} \\ \\ \mathcal{D}_R(V_A, 0) = d_R - g_{RA}^{gap} V_A \end{cases}$$

Therefore, we plot in Figure 8.A the discriminant Δ_R given in (4.5). We observe that $\Delta_R > 0$ for any value of the presynaptic membrane potential V_A. According to Proposition 4.1, the RIM postsynaptic neuron exhibits a unique stationnary point. This allows to conclude that the nature of the intrinsic dynamics of this coupled neuron remains near-linear despite the bimodality of its membrane potential. Finally, Figure 8.B shows the bistable dynamics of the synaptic activity which confers a bimodal membrane potential dynamics to the RIM neuron.

The same analysis has been conducted with the AIY neuron as the postsynaptic neuron, and AFD as the presynaptic neuron. As can be seen in Figure 10, the same results are obtained: the apparent bimodality of the AIY voltages is not the result of an intrinsic change in its nature, but of bistable synaptic inputs.

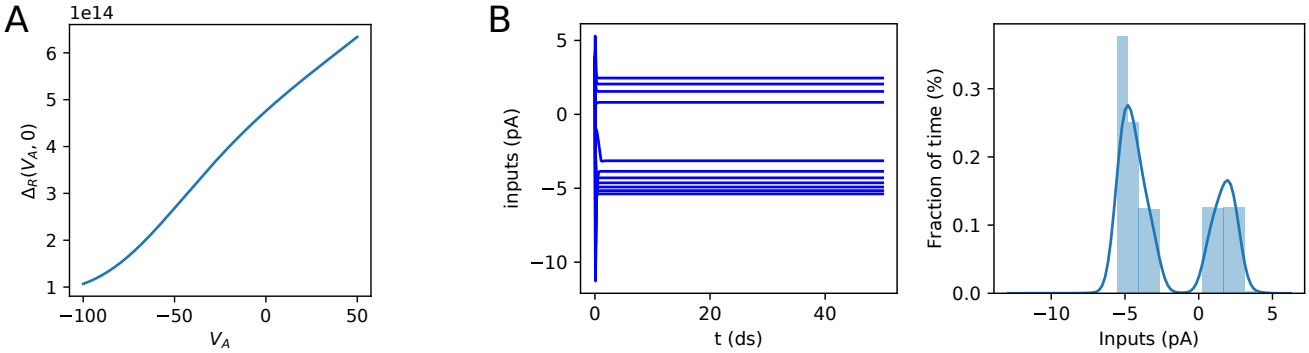

Figure 8. **(A)** Dynamics of the function $V_A \mapsto \Delta_R(V_A, 0)$. **(B)** Left: Evolution of synaptic inputs received by the RIM neuron in response to the stimulation (current injections from −15 pA to 35 pA by 5 pA increments) of the AFD presynaptic neuron. Right: Corresponding histogram of the synaptic inputs calculated from 50 ds (5000 ms) for each stimulation.

5. Conclusion and discussion

Experimental observations through calcium imaging in freely moving animals (*e.g.* in the *C. elegans* worm) show that non-spiking neural networks exhibit ON- and OFF-states. This paper aimed

at understanding how such states could emerge from the intrinsic dynamics of neurons and their couplings. To that end, we used a recently developed simple model of non-spiking neurons from which a mathematical analysis of its dynamics were carried out. In particular, we determined explicit expressions of the stationary points of the model depending on its type, near-linear or bistable. In addition, the bifurcation dynamics of the model were studied, with the determination of its normal form. Then, we determined mathematical conditions for determining whether the ON- and OFF-states in non-spiking neural networks result from the intrinsic neuron dynamics or the synaptic activity. On this basis, we highlighted that the bimodality of the membrane potential of coupled neurons could be a consequence of bistable synaptic inputs, and not of intrinsically bistable neuron dynamics contrary to what one might have expected. Further, we suggested that up- and down-states in non-spiking neural networks could be driven by bistable neurons which dictate their behaviors to their postsynaptic neurons. Such a configuration, with bistable neurons sending electrical signals to near-linear (and bistable) postsynaptic neurons, is ubiquitous in non-spiking neural networks. Indeed, many sensory, inter- and motorneurons in *C. elegans* are bistable such as ASER [9], RMD [54], AWC [55], ASH [56], AFD [33], AWA [33], AIA [57] and numerous non identified neurons [9]. In the same way, the bipolar [58] and horizontal [59] cells of the retina are bistable and send eletrical signals to ganglion and amacrine cells respectively [8]. Therefore, our study gives a rigorous framework for better understanding how the behavior of coupled non-spiking neurons depends on their intrinsic dynamics and their couplings. In particular, it allows to gain insight into how intrinsic dynamics and couplings of single non-spiking neurons impact neural network behaviors.

On the importance of distinguishing between *bimodality* and *bistability*. Here we stress the importance of distinguishing between the terms *bistable* and *bimodal*. Bistability results from the intrinsic properties of the neuron, whereas a bimodal distribution of the neuron's voltages does not necessarily. A bistable neuron inherently displays a bimodal distribution of its voltages, but a neuron can exhibit a bimodality of its voltages when it is coupled without being intrinsically bistable. Indeed, we showed in this paper that the RIM near-linear coupled neuron can display a bimodal distribution of its voltages without being transformed into a bistable neuron.

The implications on the network signal processing could be radically different whether the bimodality of the RIM voltages are induced by intrinsic bistability or not. Indeed, a modification of the near-linear type of RIM into a bistable type would endow it with new computational characteristics. In this regard, bistable neurons enhance the short-term memory capabilities of excitatory recurrent networks [60], stabilize the persistent neural activity observed in working memory systems [61], and reduce the effects of noise and distraction stimuli [57,62]. Therefore, if we want to understand the way nervous systems work to produce specific behaviors, we then must understand how synaptic activities influence the dynamics of neurons and their intrinsic nature. We argue that the current paper, through Proposition 4.1, makes this possible in the case of non-spiking networks.

Perspective. In this paper, we determined mathematical conditions to study the influence of synaptic activities on the neuron intrinsic dynamics. We applied them to canonical examples of two coupled neurons, representative of widespread configurations in non-spiking networks. However, an application on larger scale networks could be implemented in the future, for example on *C. elegans* networks for which we have the fully mapped connectome (*i.e.* the wiring diagram of its nervous system) [21,37,63].

In particular, a biological network of four pair of neurons displaying correlated up- and down-states has been well-studied in a biological viewpoint [30]. This network underlies a chemotaxis behavior, characterized by *C. elegans* reversal (reorientation) responses to odors. Modeling this network could be of significant importance to deal with many issues. For instance, a currently open question is the specific contribution of the gap junctions *vs.* chemical synapses in the emergence of the up- and down-states [30].

Acknowledgments

We thank the reviewer for their valuable comments on the manuscript, as well as Thibaut Démare, Laetitia Raison-Aubry and Sophie Bavard.

Conflict of interest

The authors declare no competing interests.

References

1. H. Markram, E. Muller, S. Ramaswamy, M. W. Reimann, M. Abdellah, C. A. Sanchez, et al., Reconstruction and simulation of neocortical microcircuitry, *Cell*, **163** (2015), 456–492. https://doi.org/10.1016/j.cell.2015.09.029
2. F. Giovannini, B. Knauer, M. Yoshida, L. Buhry, The can-in network: A biologically inspired model for self-sustained theta oscillations and memory maintenance in the hippocampus, *Hippocampus*, **27** (2017), 450–463. https://doi.org/10.1002/hipo.22704
3. F. Cavarretta, G. Naldi, Mathematical study of a nonlinear neuron model with active dendrites, *AIMS Mathematics*, **4** (2019), 831–846. https://doi.org/10.3934/math.2019.3.831
4. H. Lin, C. Wang, Y. Sun, W. Yao, Firing multistability in a locally active memristive neuron model, *Nonlinear Dynamics*, **100** (2020), 3667–3683. https://doi.org/10.1007/s11071-020-05687-3
5. H. Lin, C. Wang, Q. Deng, C. Xu, Z. Deng, C. Zhou, Review on chaotic dynamics of memristive neuron and neural network, *Nonlinear Dynamics*, **106** (2021), 959–973. https://doi.org/10.1007/s11071-021-06853-x
6. H. Lin, C. Wang, C. Chen, Y. Sun, C. Zhou, C. Xu, et al., Neural bursting and synchronization emulated by neural networks and circuits, *IEEE T. Circuits-I*, **68** (2021), 3397–3410. https://doi.org/10.1109/TCSI.2021.3081150
7. S. R. Lockery, M. B. Goodman, S. Faumont, First report of action potentials in a c. elegans neuron is premature, *Nat. Neurosci.*, **12** (2009), 365–366. https://doi.org/10.1038/nn0409-365
8. G. D. Field, E. J. Chichilnisky, Information processing in the primate retina: circuitry and coding. *Annu. Rev. Neurosci.*, **30** (2007), 1–30. https://doi.org/10.1146/annurev.neuro.30.051606.094252
9. M. B. Goodman, D. H. Hall, L. Avery, S. R. Lockery, Active currents regulate sensitivity and dynamic range in c. elegans neurons, *Neuron*, **20** (1998), 763–772. https://doi.org/10.1016/S0896-6273(00)81014-4

10. A. Roberts, B. M. H. Bush, *Neurones without impulses: their significance for vertebrate and invertebrate nervous systems*, volume 6, Cambridge University Press, 1981.

11. R. E. Davis, A. O. Stretton, Signaling properties of ascaris motorneurons: graded active responses, graded synaptic transmission, and tonic transmitter release, *J. Neurosci.*, **9** (1989), 415–425. https://doi.org/10.1523/JNEUROSCI.09-02-00415.1989

12. S. Usui, A. Ishihaiza, Y. Kamiyama, H. Ishii, Ionic current model of bipolar cells in the lower vertebrate retina, *Vision res.*, **36** (1996), 4069–4076. https://doi.org/10.1016/S0042-6989(96)00179-4

13. D. E. Kourennyi, X. D. Liu, J. Hart, F. Mahmud, W. H. Baldridge, S. Barnes, Reciprocal modulation of calcium dynamics at rod and cone photoreceptor synapses by nitric oxide, *J. Neurophysiol.*, **92** (2004), 477–483. https://doi.org/10.1152/jn.00606.2003

14. R. Publio, R. F. Oliveira, A. C. Roque, A realistic model of rod photoreceptor for use in a retina network model, *Neurocomputing*, **69** (2006), 1020–1024. https://doi.org/10.1016/j.neucom.2005.12.037

15. L. Naudin, N. Corson, M. A. Aziz-Alaoui, J. L. Jimenez Laredo, T. Démare, On the modeling of the three types of non-spiking neurons of the caenorhabditis elegans, *Int. J. Neural Syst.*, **31** (2021), 2050063. https://doi.org/10.1142/S012906572050063X

16. M. Nicoletti, A. Loppini, L. Chiodo, V. Folli, G. Ruocco, S. Filippi, Biophysical modeling of c. elegans neurons: Single ion currents and whole-cell dynamics of awcon and rmd, *PloS one*, **14** (2019), e0218738. https://doi.org/10.1371/journal.pone.0218738

17. L. Naudin, J. L. Jiménez Laredo, Q. Liu, N. Corson, Systematic generation of biophysically detailed models with generalization capability for non-spiking neurons, *PloS one*, **17** (2022), e0268380. https://doi.org/10.1371/journal.pone.0268380

18. J. L. Jiménez Laredo, L. Naudin, N. Corson, C. M. Fernandes, A methodology for determining ion channels from membrane potential neuronal recordings, *Applications of Evolutionary Computation*, (2022), 15–29. https://doi.org/10.1007/978-3-031-02462-7_2

19. J. G. White, E. Southgate, J. N. Thomson, S. Brenner, The structure of the nervous system of the nematode caenorhabditis elegans, *Philos Trans R Soc Lond B Biol Sci*, **314** (1986), 1–340. https://doi.org/10.1098/rstb.1986.0056

20. L. R. Varshney, B. L. Chen, E. Paniagua, D. H. Hall, D. B. Chklovskii, Structural properties of the caenorhabditis elegans neuronal network, *PLoS Comput. Biol.*, **7** (2011), e1001066. https://doi.org/10.1371/journal.pcbi.1001066

21. S. J. Cook, T. A. Jarrell, C. A. Brittin, Y. Wang, A. E. Bloniarz, M. A. Yakovlev, et al., Whole-animal connectomes of both caenorhabditis elegans sexes, *Nature*, **571** (2019), 63–71. https://doi.org/10.1038/s41586-019-1352-7

22. S. H. Chalasani, N. Chronis, M. Tsunozaki, J. M. Gray, D. Ramot, M. B. Goodman, et al., Dissecting a circuit for olfactory behaviour in caenorhabditis elegans, *Nature*, **450** (2007), 63–70. https://doi.org/10.1038/nature06292

23. P. Liu, B. Chen, Z. W. Wang, Gabaergic motor neurons bias locomotor decision-making in c. elegans, *Nat. commun.*, **11** (2020), 1–19. https://doi.org/10.1038/s41467-020-18893-9

24. K. T. Quach, S. H. Chalasani, Flexible reprogramming of pristionchus pacificus motivation for attacking caenorhabditis elegans in predator-prey competition, *Curr. Biol.*, **32** (2022), 1675–1688. https://doi.org/10.1101/2021.03.09.434602
25. P. Heyward, M. Ennis, A. Keller, M. T. Shipley, Membrane bistability in olfactory bulb mitral cells, *J. Neurosci.*, **21** (2001), 5311–5320. https://doi.org/10.1523/JNEUROSCI.21-14-05311.2001
26. Y. Loewenstein, S. Mahon, P. Chadderton, K. Kitamura, H. Sompolinsky, Y. Yarom, et al., Bistability of cerebellar purkinje cells modulated by sensory stimulation, *Nat. Neurosci.*, **8** (2005), 202–211. https://doi.org/10.1038/nn1393
27. S. W. Hughes, D. W. Cope, T. I. Tóth, S. R. Williams, V. Crunelli, All thalamocortical neurones possess a t-type ca2+ 'window' current that enables the expression of bistability-mediated activities, *The Journal of physiology*, **517** (1999), 805–815. https://doi.org/10.1111/j.1469-7793.1999.0805s.x
28. T. Schrödel, R. Prevedel, K. Aumayr, M. Zimmer, A. Vaziri, Brain-wide 3d imaging of neuronal activity in caenorhabditis elegans with sculpted light, *Nat. methods*, **10** (2013), 1013–1020. https://doi.org/10.1038/nmeth.2637
29. R. Prevedel, Y.-G. Yoon, M. Hoffmann, N. Pak, G. Wetzstein, S. Kato, et al., Simultaneous whole-animal 3d imaging of neuronal activity using light-field microscopy, *Nat. methods*, **11** (2014), 727–730. https://doi.org/10.1038/nmeth.2964
30. A. Gordus, N. Pokala, S. Levy, S. W. Flavell, C. I. Bargmann, Feedback from network states generates variability in a probabilistic olfactory circuit, *Cell*, **161** (2015), 215–227. https://doi.org/10.1016/j.cell.2015.02.018
31. E. M. Izhikevich, *Dynamical systems in neuroscience*, MIT press, 2007. https://doi.org/10.7551/mitpress/2526.001.0001
32. L. Naudin, J. L. Jiménez Laredo, N. Corson, A simple model of non-spiking neurons, *Neural Comput.*, **34** (2022). https://doi.org/10.1162/neco_a_01531
33. Q. Liu, P. B. Kidd, M. Dobosiewicz, C. I. Bargmann, C. elegans awa olfactory neurons fire calcium-mediated all-or-none action potentials, *Cell*, **175** (2018), 57–70. https://doi.org/10.1016/j.cell.2018.08.018
34. L. Naudin, N. Corson, M. A. A. Alaoui, A generic conductance-based model of non-spiking caenorhabditis elegans neurons and its mathematical analysis, 2021.
35. R. Storn, K. Price, Differential evolution–a simple and efficient heuristic for global optimization over continuous spaces, *J. Global Optim.*, **11** (1997), 341–359. https://doi.org/10.1023/A:1008202821328
36. R. Sarpeshkar, Analog versus digital: extrapolating from electronics to neurobiology, *Neural Comput.*, **10** (1998), 1601–1638. https://doi.org/10.1162/089976698300017052
37. J. G. White, E. Southgate, J. N. Thomson, S. Brenner, The structure of the nervous system of the nematode caenorhabditis elegans, *Philos Trans R Soc Lond B Biol Sci*, **314** (1986), 1–340. https://doi.org/10.1098/rstb.1986.0056
38. S. L. Mclntire, E. Jorgensen, J. Kaplan, H. R. Horvitz, The gabaergic nervous system of caenorhabditis elegans, *Nature*, **364** (1993), 337–341. https://doi.org/10.1038/364337a0

39. E. Serrano-Saiz, R. J. Poole, T. Felton, F. Zhang, E. D. De La Cruz, O. Hobert, Modular control of glutamatergic neuronal identity in c. elegans by distinct homeodomain proteins, *Cell*, **155** (2013), 659–673. https://doi.org/10.1016/j.cell.2013.09.052

40. L. Pereira, P. Kratsios, E. Serrano-Saiz, H. Sheftel, A. E. Mayo, D. H. Hall, et al., A cellular and regulatory map of the cholinergic nervous system of c. elegans, *Elife*, **4** (2015), e12432. https://doi.org/10.7554/eLife.12432

41. D. L. Chase, M. R. Koelle, Biogenic amine neurotransmitters in c. elegans, *WormBook: The Online Review of C. elegans Biology [Internet]*, 2007. https://doi.org/10.1895/wormbook.1.132.1

42. Z. F. Altun, B. Chen, Z.-W. Wang, D. H. Hall, High resolution map of caenorhabditis elegans gap junction proteins, *Developmental dynamics: an official publication of the American Association of Anatomists*, **238** (2009), 1936–1950. https://doi.org/10.1002/dvdy.22025

43. E. J. Jin, S. Park, X. Lyu, Y. Jin, Gap junctions: historical discoveries and new findings in the caenorhabditis elegans nervous system, *Biol. Open*, **9** (2020), bio053983.

44. Q. Liu, G. Hollopeter, E. M. Jorgensen, Graded synaptic transmission at the caenorhabditis elegans neuromuscular junction, *Proceedings of the National Academy of Sciences*, **106** (2009), 10823–10828. https://doi.org/10.1073/pnas.0903570106

45. T. H. Lindsay, T. R. Thiele, S. R. Lockery, Optogenetic analysis of synaptic transmission in the central nervous system of the nematode caenorhabditis elegans, *Nat. Commun.*, **2** (2011), 1–9. https://doi.org/10.1038/ncomms1304

46. A. Narayan, G. Laurent, P. W. Sternberg, Transfer characteristics of a thermosensory synapse in caenorhabditis elegans, *Proceedings of the National Academy of Sciences*, **108** (2011), 9667–9672. https://doi.org/10.1073/pnas.1106617108

47. P. Liu, B. Chen, Z.-W. Wang, Postsynaptic current bursts instruct action potential firing at a graded synapse, *Nat. commun.*, **4** (2013), 1–12. https://doi.org/10.1038/ncomms2925

48. W. Zou, J. Fu, H. Zhang, K. Du, W. Huang, J. Yu, et al., Decoding the intensity of sensory input by two glutamate receptors in one c. elegans interneuron, *Nat. commun.*, **9** (2018), 1–12. https://doi.org/10.1038/s41467-018-06819-5

49. R. E. Davis, A. O. Stretton, Passive membrane properties of motorneurons and their role in long-distance signaling in the nematode ascaris, *J. Neurosci.*, **9** (1989), 403–414. https://doi.org/10.1523/JNEUROSCI.09-02-00403.1989

50. R. E. Davis, A. O. Stretton, Signaling properties of ascaris motorneurons: graded active responses, graded synaptic transmission, and tonic transmitter release, *J. Neurosci.*, **9** (1989), 415–425. https://doi.org/10.1523/JNEUROSCI.09-02-00415.1989

51. S. R. Wicks, C. J. Roehrig, C. H. Rankin, A dynamic network simulation of the nematode tap withdrawal circuit: predictions concerning synaptic function using behavioral criteria, *J. Neurosci.*, **16** (1996), 4017–4031. https://doi.org/10.1523/JNEUROSCI.16-12-04017.1996

52. P. Liu, B. Chen, R. Mailler, Z.-W. Wang, Antidromic-rectifying gap junctions amplify chemical transmission at functionally mixed electrical-chemical synapses, *Nat. commun.*, **8** (2017), 14818. https://doi.org/10.1038/ncomms14818

53. Y. Shui, P. Liu, H. Zhan, B. Chen, Z.-W. Wang, Molecular basis of junctional current rectification at an electrical synapse, *Sci. Adv.*, **6** (2020), eabb3076. https://doi.org/10.1126/sciadv.abb3076

54. J. E. Mellem, P. J. Brockie, D. M. Madsen, A. V. Maricq, Action potentials contribute to neuronal signaling in c. elegans, *Nat. neurosci.*, **11** (2008), 865–867. https://doi.org/10.1038/nn.2131

55. D. Ramot, B. L. MacInnis, M. B. Goodman, Bidirectional temperature-sensing by a single thermosensory neuron in c. elegans, *Nat. neurosci.*, **11** (2008), 908–915. https://doi.org/10.1038/nn.2157

56. S. L. Geffeney, J. G. Cueva, D. A. Glauser, J. C. Doll, T. H. C. Lee, M. Montoya, et al., Deg/enac but not trp channels are the major mechanoelectrical transduction channels in a c. elegans nociceptor, *Neuron*, **71** (2011), 845–857. https://doi.org/10.1016/j.neuron.2011.06.038

57. M. Dobosiewicz, Q. Liu, C. I. Bargmann, Reliability of an interneuron response depends on an integrated sensory state, *Elife*, **8** (2019), e50566. https://doi.org/10.7554/eLife.50566

58. G. Schilardi, S. Kleinlogel, Two functional classes of rod bipolar cells in the healthy and degenerated optogenetically treated murine retina, *Front. Cell. Neurosci.*, **15** (2021). https://doi.org/10.3389/fncel.2021.809531

59. T. Aoyama, Y. Kamiyama, S. Usui, R. Blanco, C. F. Vaquero, P. de la Villa, Ionic current model of rabbit retinal horizontal cell, *Neurosci. Res.*, **37** (2000), 141–151. https://doi.org/10.1016/S0168-0102(00)00111-5

60. A. A. Koulakov, S. Raghavachari, A. Kepecs, J. E. Lisman, Model for a robust neural integrator, *Nat. neurosci.*, **5** (2002), 775–782. https://doi.org/10.1038/nn893

61. M. S. Goldman, J. H. Levine, G. Major, D. W. Tank, H. S. Seung, Robust persistent neural activity in a model integrator with multiple hysteretic dendrites per neuron, *Cereb. cortex*, **13** (2003), 1185–1195. https://doi.org/10.1093/cercor/bhg095

62. M. Camperi, X. J. Wang, A model of visuospatial working memory in prefrontal cortex: recurrent network and cellular bistability, *J. comput. neurosci.*, **5** (1998), 383–405.

63. L. R. Varshney, B. L. Chen, E. Paniagua, D. H. Hall, D. B. Chklovskii, Structural properties of the caenorhabditis elegans neuronal network, *PLoS Comput. Biol.*, **7** (2011), e1001066. https://doi.org/10.1371/journal.pcbi.1001066

Appendix

A. Supplementary materials

Table 2. Parameter values of the model (2.1) for the RIM, AIY and AFD neurons.

Parameters / Neuron	a	b	c	d	$\tau\ (10^{-1}s)$
RIM	0.000024	0.0036	0.31	7.22	0.042
AIY	0.000044	0.0093	0.773	20.38	0.04
AFD	0.00033	0.048	2.31	38.99	0.06

B. Supplementary figures

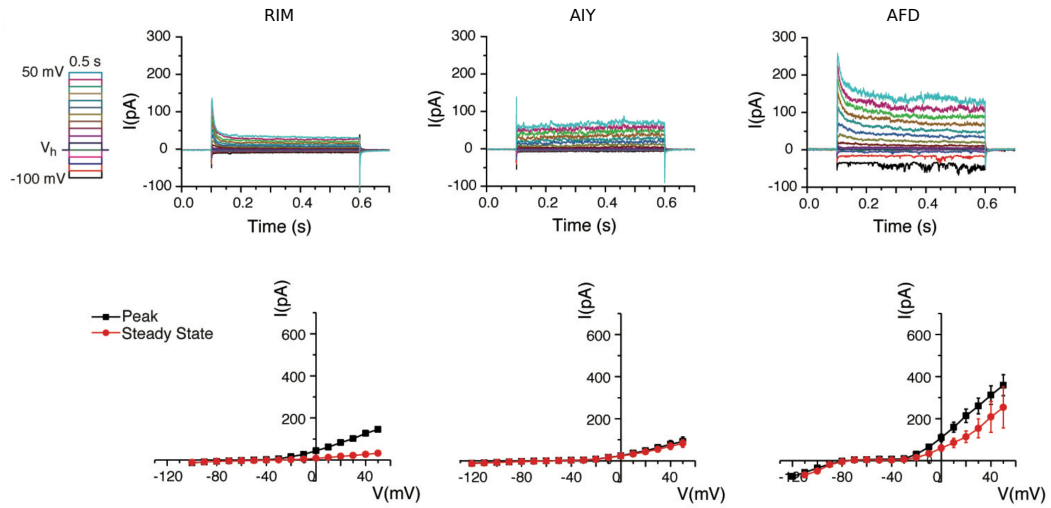

Figure 9. (Top) Evolution of the total ion currents of the RIM, AIY and AFD neurons for different fixed values of their membrane potentials, starting from −100 mV and increasing to 50 mV by 10 mV increments. (Bottom) Current-membrane relationships obtained from averaged voltage-clamp recordings (RIM: $n = 3$; AIY: $n = 7$; AFD: $n = 3$); see Figure 2.A for detailed explanations about how to obtain this relationship from (Top). Peak currents are measured by the absolute maximum amplitude of currents within the first 100 ms of each voltage step onset, while steady-state currents are measured by the averaged currents of the last 50 ms of each voltage step. The figure has been reproduced from [33] with the consent of the authors.

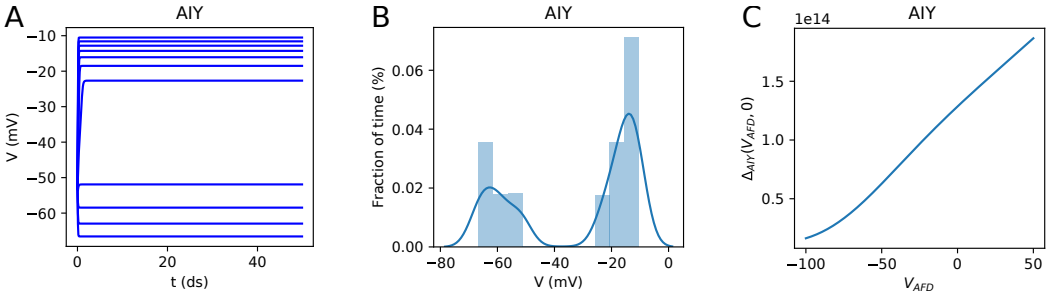

Figure 10. **(A)** Evolution of the membrane potential of the AIY neuron when its AFD bistable presynaptic neuron is stimulated by a series of injection currents I^{ext}, from −15 pA to 35 pA by 5 pA increments. **(B)** Corresponding histogram of the membrane potential calculated from 50 ds (5000 ms) of simulation. **(C)** Dynamics of the function $V_{AFD} \mapsto \Delta_{AIY}(V_{AFD}, 0)$.